ACS APPLIED MATERIALS & INTERFACES

Research Article

www.acsami.org

Influence of Metal–MoS_2 Interface on MoS_2 Transistor Performance: Comparison of Ag and Ti Contacts

Hui Yuan,*[†,‡] Guangjun Cheng,*[†] Lin You,[†] Haitao Li,[†,‡] Hao Zhu,[†,‡] Wei Li,[†] Joseph J. Kopanski,[†] Yaw S. Obeng,[†] Angela R. Hight Walker,[†] David J. Gundlach,[†] Curt A. Richter,[†] Dimitris E. Ioannou,[‡] and Qiliang Li*[‡]

[†]Semiconductor and Dimensional Metrology Division, National Institute of Standards and Technology, Gaithersburg, Maryland 20878, United States

[‡]Department of Electrical and Computer Engineering, George Mason University, Fairfax, Virginia 22030, United States

Supporting Information

ABSTRACT: In this work, we compare the electrical characteristics of MoS_2 field-effect transistors (FETs) with Ag source/drain contacts with those with Ti and demonstrate that the metal–MoS_2 interface is crucial to the device performance. MoS_2 FETs with Ag contacts show more than 60 times higher ON-state current than those with Ti contacts. In order to better understand the mechanism of the better performance with Ag contacts, 5 nm Au/5 nm Ag (contact layer) or 5 nm Au/5 nm Ti film was deposited onto MoS_2 monolayers and few layers, and the topography of metal films was characterized using scanning electron microscopy and atomic force microscopy. The surface morphology shows that, while there exist pinholes in Au/Ti film on MoS_2, Au/Ag forms a smoother and denser film. Raman spectroscopy was carried out to investigate the metal–MoS_2 interface. The Raman spectra from MoS_2 covered with Au/Ag or Au/Ti film reveal that Ag or Ti is in direct contact with MoS_2. Our findings show that the smoother and denser Au/Ag contacts lead to higher carrier transport efficiency.

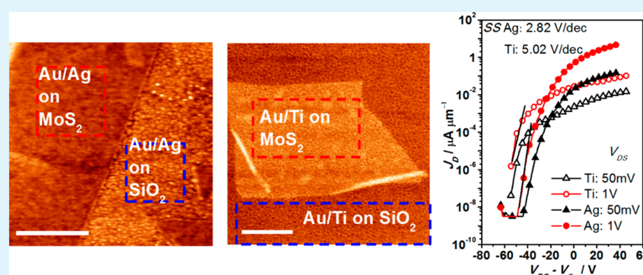

KEYWORDS: *2D material, metal contact, Raman spectroscopy, field-effect transistor, transition-metal dichalcogenides, molybdenum disulfide*

INTRODUCTION

Recently, MoS_2 has attracted a lot of attention for its electronic and optoelectronic applications.[1−5] Layered MoS_2 is a two-dimensional (2D) semiconductor which has a band gap ranging from 1.2 to 1.8 eV depending on its thickness.[6−8] In particular, monolayer MoS_2 with a direct band gap of 1.8 eV shows promising applications in optoelectronics.[8−10] Two-dimensional MoS_2 is also attractive for flexible electronic applications because of its intrinsic ultrathin body and robust lattice structure.[11−13] Considering short channel effects in metal–oxide–semiconductor field effect transistors (MOSFETs), this intrinsic ultrathin body also represents the ultimate in scaling.[14] Moreover, its inert surface has no dangling bonds, which is advantageous for forming the channel–gate dielectric interface in MOSFETs. Monolayer MoS_2 MOSFET was the first demonstrated 2D transition-metal dichalcogenide semiconductor MOSFET.[15] Such transistors have exhibited a high ON/OFF ratio of 10^8 and decent subthreshold slopes of 74 mV/dec which is compatible with current state-of-the-art CMOS technology.

Various work has been done to understand the transport mechanism in MoS_2 transistors and to improve their performance for future applications.[16−21] The source/drain (S/D) contacts are very important factors for device performance. A variety of contacts have been used and studied to achieve a good Ohmic contact to MoS_2.[13,22−26] It was originally expected that a low work function metal may lead to a lower Schottky barrier for electron transport and result in a good n-type contact.[22] However, the experimental results from Das et al. show that the barrier height between the MoS_2 channel and the metal contact is only weakly influenced by the metal work function and that an n-type barrier even forms between MoS_2 and high-work function metal such as Pt.[22] The theoretical work by Gong et al. confirms that partial Fermi level pinning in metal–MoS_2 contacts makes the Fermi levels in all studied metal–MoS_2 complexes except Pt situated above the midgap of MoS_2.[23] Additionally, McDonnell et al. demonstrate that intrinsic defects in MoS_2 dominate the metal–MoS_2 contact resistance and provide a low Schottky barrier independent of the metal contact work function.[24] All these complications show that metal work function is not a good indicator for forming an Ohmic contact between metal and MoS_2.

Received: October 8, 2014
Accepted: December 16, 2014
Published: December 16, 2014

ACS Publications © 2014 American Chemical Society

Previous studies on metal contacts to graphene or carbon nanotube demonstrate that the morphology of metal contacts and the interaction between these carbon materials and metal contacts play important roles in contact resistance.[26,27] Although it is well believed that metal wettability plays an important role in metal−MoS_2 contacts,[22] to our best knowledge, there is no work showing direct evidence on how the metal contact morphology affects the metal−MoS_2 contacts. In this work, for the first time, we have shown how the metal−MoS_2 interface influences the MoS_2 FET performance.

Ag was chosen because it has been reported to form a good contact on WSe_2,[28] which is a material similar to MoS_2. Previous work also shows that Ag has excellent wettability on bulk MoS_2.[29,36,37] We compare the results from Ag contacts with those from Ti contacts, which are commonly used metal contacts with MoS_2 in the literature.[10,15,22,30−33] Our results show that, despite the similar work function around 4.3 eV for both metals,[34] monolayer and few-layer MoS_2 transistors with Ag contacts show significantly better electrical characteristics with more than 60 times higher ON-state current density.

The surface morphology of the metal films was then investigated by depositing a 5 nm thin layer of contact metal (Ag or Ti) capped with a 5 nm Au protection layer on top of MoS_2. Scanning electron microscopy (SEM) shows that a smoother and denser Au/Ag film is formed on top of MoS_2. The surface roughness analysis was carried out by atomic force microscopy (AFM). The metal−MoS_2 interface was then investigated by Raman spectroscopy, and the Raman spectra reveal that the contacting interface is between MoS_2 and Ag or Ti. The better wettability between Ag and MoS_2 is essential to forming smoother and denser Au/Ag contacts on MoS_2, resulting in a better device performance. The strain effect introduced by Ag and heating effect introduced by Ti to monolayer MoS_2 are also revealed by Raman spectroscopy.

RESULTS AND DISCUSSION

Electrical Characterization of MoS_2 Transistors. Our devices were fabricated with exfoliated MoS_2 on 280 nm SiO_2/Si substrate. We deposited 30 nm Au/30 nm Ag for Ag contacted MoS_2 FETs and 30 nm Au/30 nm Ti for Ti contacted ones by electron-beam evaporation. The resulting devices have a channel length of 1 μm and a contact width of 1 μm as well (Figure 1a). In total, five devices with Ag contacts (one monolayer and four few layer) and six devices with Ti contacts (four monolayer and two few layer) were measured.

Figure 1b−d shows the representative electric characteristics of monolayer MoS_2 transistors. We normalized the drain current (I_D) to the current density per 1 μm channel width (J_D) to compare the electrical characteristics of transistors with different channel widths. Figure 1b compares the characteristics of J_D versus back-gate voltage (V_{BG}) (J_D−V_{BG} characteristics) in monolayer MoS_2 transistors with Ag and Ti contacts. The devices were tested with V_{BG} varying from −100 to 0 V and drain to source voltage (V_{DS}) equal to 50 mV or 1 V. All our devices show n-type MOSFET behaviors. The threshold voltage of the devices was extracted from the linear fitting of the ON-state current versus V_{BG} with V_{DS} = 50 mV. The device threshold voltages are equal to −36.6 and −45.4 V for Ag and Ti contacts, respectively. These results are reasonable since Ag and Ti have similar work functions. The devices with Ti contacts show a typical ON-state current density, which is comparable to other back-gated MoS_2 transistors without high-

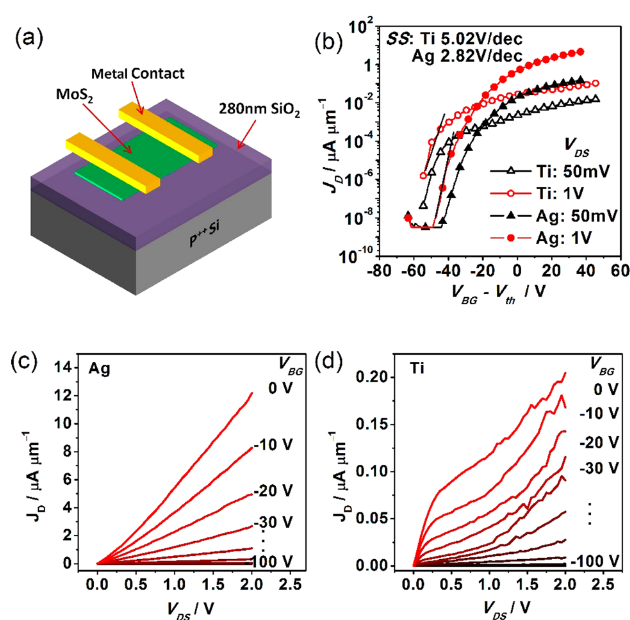

Figure 1. (a) Device diagram and drain current density of single-layer MoS_2 transistors versus (b) $V_G - V_{th}$ with Ag or Ti contacts, and (c, d) drain voltage (V_{DS}) with (c) Ag or (d) Ti contacts.

k dielectric passivation.[30−32] Most importantly, the devices with Ag contacts exhibit almost 2 orders of magnitude larger ON-state current density than those with Ti contacts. We extracted subthreshold slope (SS) of the devices, which is given by

$$SS = \left. \frac{dV_{BG}}{d(\log(I_D))} \right|_{V_{DS}} \quad (1)$$

SS was extracted from J_D−V_{BG} characterization at V_{DS} = 1 V. For devices with Ag contacts, the SS is 2.82 V/dec, and with Ti contacts, it is 5.02 V/dec. A similar SS value was also reported in the back-gated MoS_2 FETs in previous publications.[30,32] These large SS values are due to the large thickness (280 nm) of back-gate oxide.

Parts c and d of Figure 1 compare J_D−V_{DS} (source−drain voltage) characteristics of monolayer MoS_2 FETs with Ag and Ti contacts, respectively. The drain current was measured with V_{DS} varying from 0 to 2 V with V_{BG} varying from 0 to −100 V with a −10 V step. In Figure 1c, the superlinear relationship between ON-state J_D and V_{DS} near zero in monolayer MoS_2 FETs with Ag contacts indicates the Schottky barrier transistor behavior. In Figure 1d, the ON-state current density of MoS_2 FETs with Ti contacts is consistent with previous publications,[30,32] and significantly smaller than the ones with Ag contacts. The linear dependence of J_D on V_{DS} could be a result of thermally assisted tunneling, and may not necessarily indicate an Ohmic contact.[22] The current density of monolayer MoS_2 FET with Ag contacts is 60 times larger at V_{BG} = 0 V and V_{DS} = 2 V than that with Ti contacts. This larger magnitude of ON-state current density reflects the higher carrier injection efficiency.

Figure 2 shows representative electrical properties of few-layer (two to three layers) MoS_2 FETs. The drain current in these few-layer MoS_2 FETs was measured under the same bias conditions as the monolayer devices. In Figure 2a, J_D−V_{BG} characteristics of few-layer MoS_2 FETs with Ag and Ti contacts were compared. All the devices show n-type MOSFET

DOI: 10.1021/am506921y
ACS Appl. Mater. Interfaces 2015, 7, 1180−1187

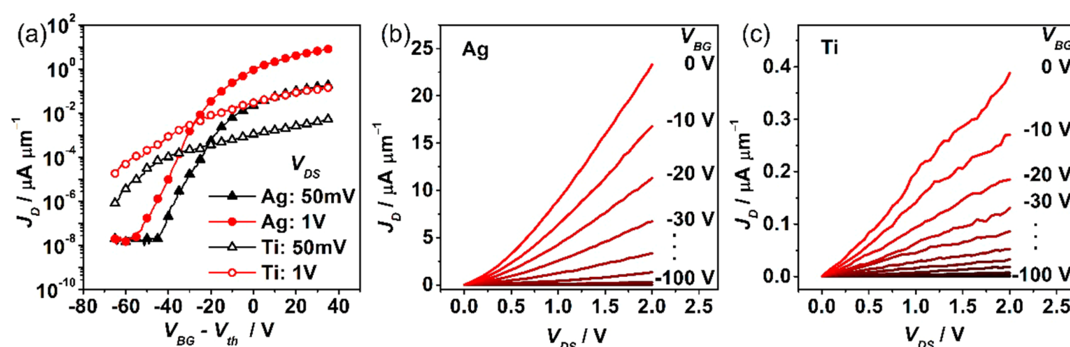

Figure 2. Drain current density of few-layer MoS_2 transistors versus (a) $V_G - V_{th}$ with Ag or Ti contacts, and (b, c) drain voltage (V_D) with (b) Ag or (c) Ti contacts.

behavior. The threshold voltage is −35.0 V for devices with Ag and Ti contacts. The subthreshold slope of transistors with Ag contacts is 5.42 V/dec. The devices with Ti contacts also show typical performance reported in previous publications.[30−32] The few-layer MoS_2 transistors with Ti contacts cannot be turned off completely even at V_{BG} = −100 V. Therefore, the subthreshold slope cannot be precisely extracted. Nonetheless, the comparison between these two devices does show improved current density and subthreshold slope with the Ag contacts.

Parts b and c of Figure 2 show J_D−V_{DS} characteristics of few-layer MoS_2 FETs with Ag and Ti contacts, respectively. Similar to monolayer MoS_2 FETs, a 60-time ON-state current enhancement is also shown in few-layer MoS_2 FETs with V_{BG} = 0 V and V_{DS} = 2 V.

In general, all our transistors with Ag contacts have much higher ON-state current density than those with Ti contacts (see Supporting Information, Figure S1). As the contacting metal, Ag or Ti, is thick enough, the barrier height between MoS_2 and metal is dominated by the interaction between MoS_2 and the direct contact metal layer. Here, Ag and Ti have very similar work functions (4.26 eV for Ag and 4.33 eV for Ti).[34] Interestingly, theoretical simulations have shown that Ti is a better contact with WSe_2 than Ag,[28,33] but experimental results show that the devices with Ag contacts perform much better than those with Ti.[28] To gain a better understanding, we performed the surface and interface characterization on our metal contacts.

Surface Morphology of Metal Thin Films on MoS_2. To understand the performance difference, we deposited 5 nm of Ag or 5 nm of Ti on top of exfoliated MoS_2 followed by the deposition of 5 nm of Au as a protection layer. The conditions used are the same with device fabrication except that the deposition rate was kept at ≈0.2 Å/s for the whole metal deposition process to mimic the device fabrication.

Then, scanning electron microscopy (SEM) was carried out to characterize their surface morphology. From SEM images (Figure 3), the morphologies of Au/Ag and Au/Ti films on MoS_2 are found to be significantly different. Figure 3a shows that the Au/Ag morphology on MoS_2 and on SiO_2/Si substrate is so distinct that the MoS_2 area can be clearly identified. Au/Ag forms surprisingly a much smoother and denser film on MoS_2 than on SiO_2/Si. In contrast, with the appearance of pinholes, Au/Ti film shows quite similar morphologies on both MoS_2 and SiO_2/Si (Figure 3b). Therefore, the location of monolayer MoS_2 is very difficult to identify, though we can still identify it through its edges.

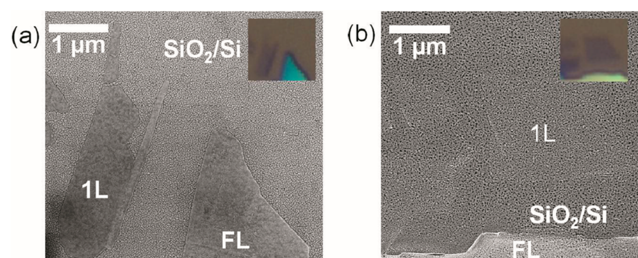

Figure 3. SEM images of MoS_2 on SiO_2/Si substrate after (a) Au/Ag deposition and (b) Au/Ti deposition. The insets show corresponding optical image of as-exfoliated MoS_2 before metal deposition. The locations of monolayer MoS_2 (1L) and few-layer MoS_2 (FL) are identified after metal deposition.

Atomic force microscopy (AFM) was used to further analyze the surface roughness of the metal films. As seen in the AFM images (Figure 4), topography of the metals on MoS_2 and SiO_2/Si substrate exhibits significant differences. Au/Ag on MoS_2 is smoother than on SiO_2/Si (Figure 4a). A line profile shows that the surface of Au/Ag on monolayer MoS_2 is 0.54 nm lower than on SiO_2/Si on average (Figure 4b), providing additional evidence of the formation of a smoother and denser metal film (Au/Ag) on MoS_2. The normalized height histograms of Au/Ag show a narrower height distribution on MoS_2 than on SiO_2/Si (Figure 4c). The root-mean-squared (RMS) surface roughness is 0.37 nm on MoS_2, but 0.61 nm on SiO_2/Si. For Au/Ti, however, pinholes are clearly seen on both MoS_2 and SiO_2/Si (Figure 4d). The surface of Au/Ti on MoS_2 is 2.18 nm higher than that on SiO_2/Si (Figure 4e). The difference between the two surfaces is much higher than the thickness of monolayer MoS_2, probably indicating the thickness difference between metal−MoS_2 and metal−SiO_2 interfaces. The metal surface roughness is almost the same on MoS_2 and on SiO_2/Si (Figure 4f): RMS roughness is 1.08 nm and 1.09 nm on MoS_2 and on SiO_2/Si, respectively. Clearly, the Au/Ag film is much smoother than the Au/Ti film on MoS_2.

Raman Spectroscopy of MoS_2 Covered with Metal. Recently, Raman spectroscopy has been used to investigate the effects of the metal−MoS_2 interface on the electronic and phonon properties of MoS_2.[35] We carried out our Raman spectroscopy measurements on monolayer and few-layer MoS_2 before and after deposition of the thin metal films (5 nm Au/5 nm Ag or 5 nm Au/5 nm Ti).

Figure 5 shows the representative Raman spectra of MoS_2 before and after metal deposition. Before metal deposition, the Raman spectrum of the as-exfoliated MoS_2 shows E^1_{2g} (an in-

DOI: 10.1021/am506921y
ACS Appl. Mater. Interfaces 2015, 7, 1180−1187

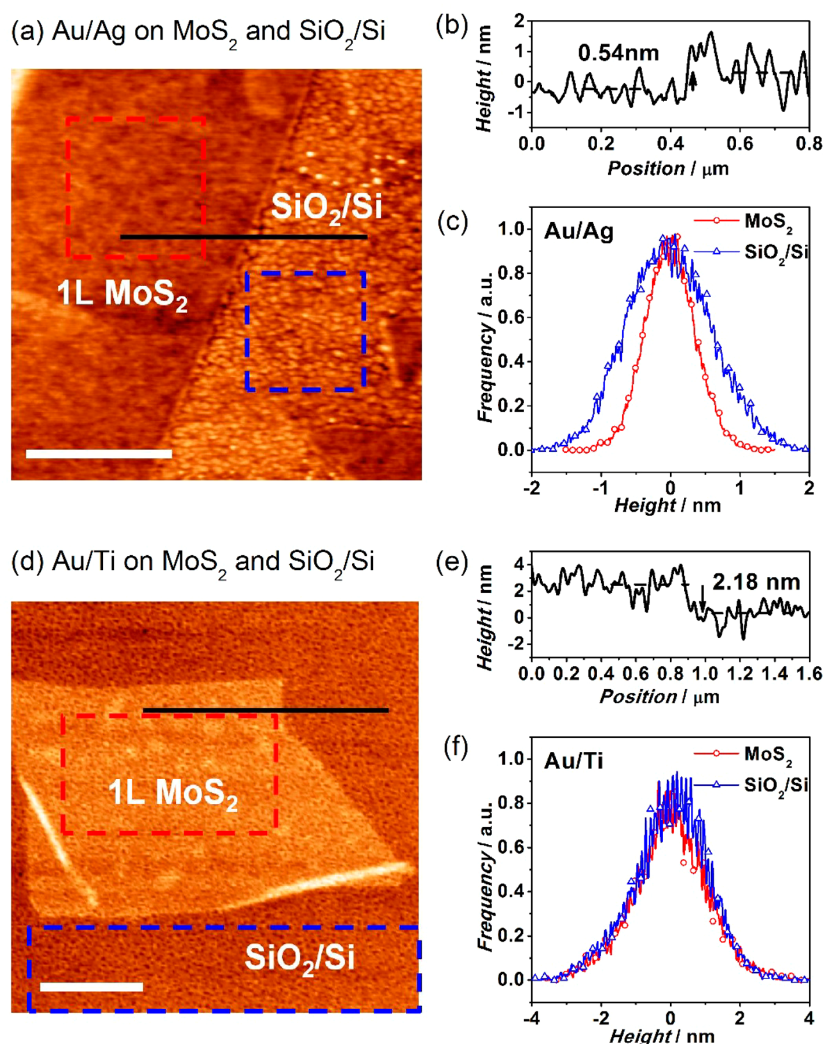

Figure 4. AFM and roughness analysis of metal on MoS_2 and SiO_2/Si substrate: (a) topography of Au/Ag on MoS_2 and SiO_2/Si. (b) Topographic line profile of the height along the slide line indicated in (a). (c) Normalized histograms of height distribution of areas indicated by the squares in (a). (d) Topography of Au/Ti on MoS_2 and SiO_2/Si. (e) Topographic line profile of the height along the slide line indicated in (d). (f) Normalized histograms of height distribution of areas indicated by the rectangles in (d). Scale bars are 500 nm long for (a) and (d).

plane lattice vibration mode) and A_{1g} (an out-of-plane vibration mode) peaks (Figure 5a). These two peaks are symmetric, and each is fitted well with a single Lorentz peak. For as-exfoliated monolayer MoS_2, the Raman shift difference between these two peaks is 18.6 cm^{-1} for the Au/Ag sample and 18.3 cm^{-1} for the Au/Ti sample (Figure 5a,b). After Au/Ag deposition, there is no significant change in peak position for the A_{1g} mode (Figure 5a). However, the E^1_{2g} mode of MoS_2 splits into two peaks with a separation of 6.6 cm^{-1}. Also the higher frequency peak of the E^1_{2g} mode has a 0.7 cm^{-1} red shift compared to as-exfoliated monolayer MoS_2. The more significant effects of Au/Ag deposition on the E^1_{2g} mode indicate that the metal deposition affects the in-plane lattice vibration more than the out-of-plane. Gong et al. compared Raman spectra of monolayer MoS_2 with different metal depositions,[35] and their results show stronger effects on the E^1_{2g} mode than on the A_{1g} mode by Au and Ag deposition. In Ag covered monolayer MoS_2, the E^1_{2g} peak splits into two peaks. The peak at higher frequency remains in the same position with the E^1_{2g} peak of as-exfoliated MoS_2 and the other has a 6.38 cm^{-1} red shift.[35] But, in their Au covered monolayer MoS_2, the E^1_{2g} peak is broadened and has a red shift with only a 3.8 cm^{-1} peak split.[35] In our Au/Ag covered monolayer MoS_2, the E^1_{2g} peak split is 6.6 cm^{-1} and the peak at high frequency has a very little red shift compared to the as-exfoliated monolayer MoS_2. This peak splitting is very similar to the Ag covered monolayer MoS_2 sample observed by Gong et al.[35] It indicates that, in our sample, Au does not penetrate through Ag to make a direct contact with MoS_2 and Ag is indeed the contact metal.

After the deposition of Au/Ti film on monolayer MoS_2, both E^1_{2g} and A_{1g} peaks show a red shift and are broadened significantly (Figure 5b). However, each peak still remains symmetric and can be fitted with a single Lorentz peak. The Raman spectra from four different spots on Au/Ti covered monolayer MoS_2 show consistent changes in peak positions (see Supporting Information, Figure S2). Even though there are pinholes in Au/Ti film on MoS_2, on the basis of the work by Gong et al.,[35] the absence of E^1_{2g} peak splitting indicates that the contacting layer is Ti instead of Au.

We can now explain the dramatic topographic difference between Au/Ag and Au/Ti films on MoS_2. It is reasonable to correlate this difference with the roughness of the contact layer. Raman spectroscopy reveals that the contact layer with MoS_2 is Ag and Ti for Au/Ag and Au/Ti films, respectively. As a result,

DOI: 10.1021/am506921y
ACS Appl. Mater. Interfaces 2015, 7, 1180−1187

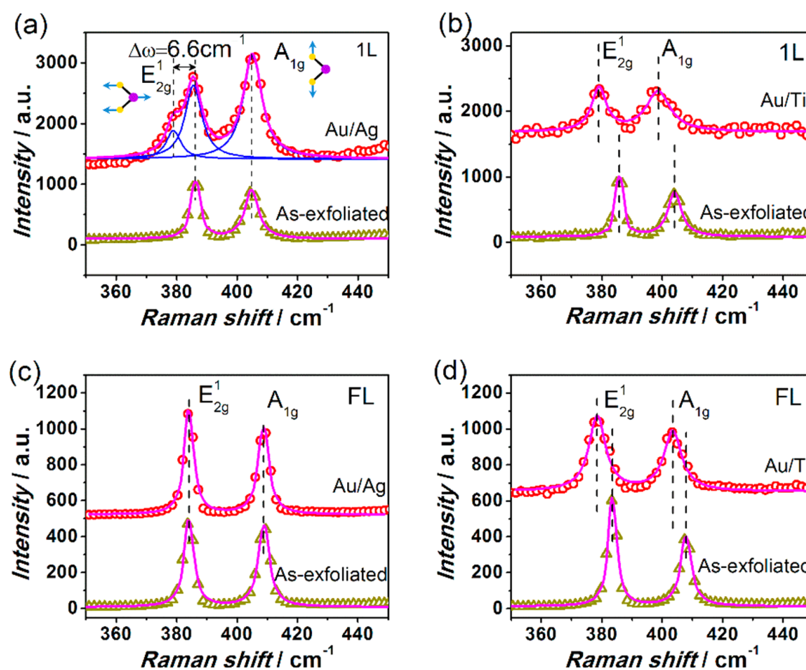

Figure 5. Comparison of Raman spectra before and after (a) Au/Ag or (b) Au/Ti deposition on monolayer (1L) MoS_2 and before and after (c) Au/Ag or (d) Au/Ti deposition on few-layer (FL) MoS_2. The symbols are real data, and solid lines are fitted Lorentz peaks.

the smoother topography observed with the Au/Ag film indicates the smoother Ag contacting layer with MoS_2. Ag has exhibited a good wettability on bulk MoS_2.[29,36−38] Our results show that this good wettability is preserved on monolayer and few-layer MoS_2 as well.

As we did not anneal our devices for the electrical measurements, the performance difference cannot be simply attributed to the chemical reaction between Ag and MoS_2 because previous work has shown that Ag does not react with MoS_2 at room temperature.[37] Meanwhile, previous work has shown that even the exfoliated MoS_2 has defects.[24] These defects could play important roles during the growth of Ag film on MoS_2 and provide active sites for the chemical reaction between Ag and MoS_2. The inhomogeneity in the defect distribution could also contribute to the performance variations among our MoS_2 transistors. Since, in general, our MoS_2 transistors with Ag contacts exhibit much higher ON-state current (see Supporting Information, Figure S1), we can conclude that the MoS_2 FET performance is enhanced by the better contacting interface between Ag and MoS_2.

The E^1_{2g} peak splitting in the Au/Ag covered monolayer MoS_2 is the result of the in-plane strain introduced by metal deposition. Previous studies[35,39,40] demonstrated the influence of uniaxial tensile strain on MoS_2 phonon modes. Their results showed that the out-of-plane A_{1g} mode was not shifted by strain while the in-plane E^1_{2g} mode was split 4.5 cm^{-1} by 1% strain. Therefore, we estimate that the Au/Ag film introduces 1.46% strain into our MoS_2 sample (6.6 cm^{-1} ÷ (4.5 cm^{-1}/1%) = 1.46%). In contrast to monolayer MoS_2, few-layer MoS_2 did not show such significant changes in the Raman spectrum after Au/Ag deposition (Figure 5c) and both peaks stay at almost the same positions. Castellanos-Gomez et al. studied the localized uniaxial strain influences on the few-layer MoS_2 Raman spectra.[41] They found that, in few-layer (three to five layers) MoS_2, both E^1_{2g} and A_{1g} modes show a red shift with strain, whereas the E^1_{2g} mode shifts larger, about 1.7 cm^{-1} per 1% strain. The absence of the peak shift in our Au/Ag covered few-layer MoS_2 indicates that the tensile strain introduced by metal deposition might be thickness dependent.

On the monolayer MoS_2 after Au/Ti deposition, the E^1_{2g} peak has a 6.7 cm^{-1} red shift and the A1g peak has a 5.5 cm^{-1} red shift (Figure 5b). The simultaneous peak shifts of E^1_{2g} and A_{1g} modes clearly indicate the temperature increase in the samples during the Raman measurement. The Raman modes of monolayer MoS_2 affected by temperature have been investigated in the literature: Both E^1_{2g} and A_{1g} peaks show a red shift when temperature increases.[42−46] From the red shifts of both peaks in our samples, the temperature of Ag/Ti covered monolayer MoS_2 increased significantly during the Raman measurement. This heating effect was also observed in the Raman spectrum of few-layer MoS_2: the two peaks also show a red shift simultaneously after Au/Ti film deposition (Figure 5d). The peak red shifts are 5.0 cm^{-1} for the E^1_{2g} mode and 4.2 cm^{-1} for the A_{1g} mode.

The temperature increase in Au/Ti coated MoS_2 is due to the laser heating during Raman measurement. To confirm this, we performed Raman measurements with different powers and signal collection times on monolayer MoS_2 covered by thin layer Au/Ti (Figure 6). When the power is as low as 10% of the total laser power, and the signal collection time is 10 s, no significant peak shift is observed. However, as the laser power increases or the signal collection time gets longer, the peak shift becomes more significant. This indicates that the peak shift is a result of the laser heating of the sample.

It is interesting to realize that the heating effect is not seen in as-exfoliated and Au/Ag covered MoS_2. The dramatic difference in thermal conductivity between Ag and Ti could contribute to the difference in heating effect between Au/Ag covered MoS_2 samples and Au/Ti covered ones. At room temperature, the thermal conductivity of Ag is almost 20 times larger than that of Ti.[47] The higher thermal conductivity of Ag and the smoother and denser morphology of the Ag film enhance the heat dissipation efficiency. Therefore, the heating effect is weaker in Au/Ag covered MoS_2 samples. We also notice that the heating

DOI: 10.1021/am506921y
ACS Appl. Mater. Interfaces 2015, 7, 1180−1187

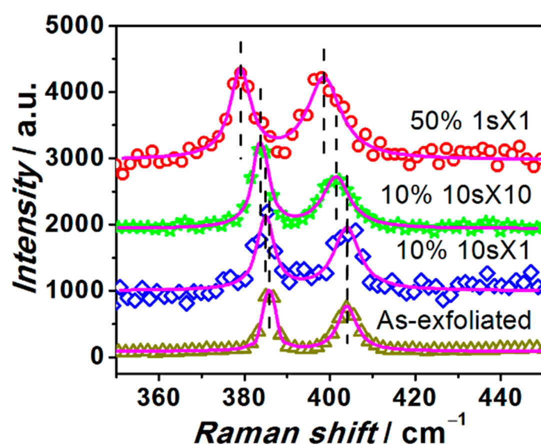

Figure 6. Raman spectra on Au/Ti covered MoS_2 with different powers and signal collection times. Symbols are experimental data, and solid lines are fitted curves.

effect occurs on on monolayer and few-layer MoS_2 covered with Au/Ti. On the thicker MoS_2, the heating effect is not significant. This phenomenon probably is related to the strong photoluminescence from monolayer and few-layer MoS_2 and its interaction with Ti under ambient conditions.

■ CONCLUSION

In summary, both monolayer and few-layer MoS_2 FETs with Ag source/drain contacts show 60 times larger ON-state current than those with Ti contacts. SEM and AFM both show that the topography of Au/Ag film on MoS_2 is significantly smoother and denser than that of Au/Ti film. Raman spectroscopy revealed that the contact layers are Ag and Ti in these two cases. It is reasonable to conclude that the smoother and denser Ag contact leads to higher carrier transport efficiency, and is the main reason for the performance enhancement. Also, the high thermal conductivity can be a benefit for the heat dissipation during device operation. Considering that proper source/drain metal contacts are crucial for forming higher quality MoS_2 transistors, our result indicates that the metal/MoS_2 interface morphology is a crucial parameter to consider when optimizing electrical contacts.

■ EXPERIMENTAL METHODS

Sample Preparation. The sample preparation started with exfoliating bulk MoS_2 (SPI small crystals) into monolayer and few-layer films on 280 nm SiO_2/Si. The MoS_2 film thickness was confirmed by the color, Raman spectroscopy, and AFM. The MoS_2 flake positions were identified with predesigned alignment marks by an optical microscope. Fabrication of back-gated MoS_2 FETs starts with patterning the source/drain contacts with electron-beam lithography and metal deposition. We deposited 30 nm Au/30 nm Ag for Ag contacted MoS_2 FETs and 30 nm Au/30 nm Ti for Ti contacted ones as the contact metals by e-beam evaporation. The system pressure was kept at $\approx 1 \times 10^{-6}$ Torr during the metal deposition. The first 5 nm of metal which directly contacted to MoS_2 was deposited at a lower rate of ≈0.2 Å/s to improve the interface roughness, and rest of the metal was deposited at a higher rate of ≈1 Å/s. The metal deposition rate and film thickness were measured in situ with a crystal sensor installed in the e-beam evaporator (Denton Vacuum Infinity 22 electron beam evaporator). The resulting devices have a channel length of 1 μm and contact width of 1 μm as well.

Samples for SEM, AFM, and Raman spectroscopy were prepared in the same way except there was no e-beam lithography step and the thickness of metal deposited was thinner. The 5 nm Au/5 nm Ag and 5 nm Au/5 nm Ti were deposited by e-beam evaporation. The conditions used were the same with device fabrication except that the deposition rate was kept at ≈0.2 Å/s for the whole metal deposition process to mimic the device fabrication.

Characterizations. The MoS_2 FETs were tested in a vacuum probe station. The system was kept at $\approx 1 \times 10^{-6}$ Torr during the measurement. A semiconductor parameter analyzer (HP 4156C) was used to carry out the electric measurement. SEM was done with a Zeiss Ultra-60 Field Emission SEM. An accelerate voltage of 5 kV was used to capture the images. AFM images were taken with Dimension system controlled by a Nanoscope V (Bruker, Santa Barbara, CA). All AFM experiments were performed with a SCANASYST-AIR tip (Bruker, Santa Barbara, CA) with a radius of 10 nm. AFM data were analyzed with WSxM software.[48] Raman spectra were acquired under ambient conditions with a micro-Raman spectrometer (Renishaw InVia Raman system) equipped with a 514.5 nm (2.41 eV) wavelength excitation laser and an 1800 lines/mm grating while operating in 180° backscattering geometry. A 50× objective was used to focus the excitation laser to an approximately 1 μm spot onto the sample. The 100% laser power was 4.8 mW. We typically used 50% power to collect the signal for 1 s to compare the Raman spectra before and after metal deposition.

■ ASSOCIATED CONTENT

Supporting Information

Statistics of ON-state current of MoS_2 transistors which is measured at $V_G = 0$ V and $V_D = 1$ V, and Raman spectra of monolayer MoS_2 covered by 5 nm Au/5 nm Ti measured at four different points. This material is available free of charge via the Internet at http://pubs.acs.org.

■ AUTHOR INFORMATION

Corresponding Authors

*E-mail: hyuan@gmu.edu.
*E-mail: guangjun.cheng@nist.gov.
*E-mail: qli6@gmu.edu.

Author Contributions

The manuscript was written through contributions of all authors. All authors have given approval to the final version of the manuscript.

H.Y. and G.C. contributed equally.

Funding

This work was supported in part by U.S. NIST Grant 60NANB11D148, the U.S. NSF grant ECCS-1407807 and ECCS-1127093.

Notes

The authors declare no competing financial interest.

■ ACKNOWLEDGMENTS

Research was performed in part at the NIST Center for Nanoscale Science and Technology. We identify certain commercial equipment, instruments, or materials in this article to specify adequately the experimental procedure. In no case does such identification imply recommendation or endorsement by the National Institute of Standards and Technology, nor does it imply that the materials or equipment identified are necessarily the best available for the purpose.

■ REFERENCES

(1) Butler, S. Z.; Hollen, S. M.; Cao, L.; Cui, Y.; Gupta, J. A.; Gutiérrez, H. R.; Heinz, T. F.; Hong, S. S.; Huang, J.; Ismach, A. F.; Johnston-Halperin, E.; Kuno, M.; Plashnitsa, V. V.; Robinson, R. D.; Ruoff, R. S.; Salahuddin, S.; Shan, J.; Shi, L.; Spencer, M. G.; Terrones, M.; Windl, W.; Goldberger, J. E. Progress, Challenges, and

DOI: 10.1021/am506921y
ACS Appl. Mater. Interfaces 2015, 7, 1180−1187

Opportunities in Two-Dimensional Materials Beyond Graphene. *ACS Nano* **2013**, *7*, 2898−2926.
(2) Jariwala, D.; Sangwan, V. K.; Lauhon, L. J.; Marks, T. J.; Hersam, M. C. Emerging Device Applications for Semiconducting Two-Dimensional Transition Metal Dichalcogenides. *ACS Nano* **2014**, *8*, 1102−1120.
(3) Roy, T.; Tosun, M.; Kang, J. S.; Sachid, A. B.; Desai, S. B.; Hettick, M.; Hu, C. C.; Javey, A. Field-Effect Transistors Built from All Two-Dimensional Material Components. *ACS Nano* **2014**, *8*, 6259−6264.
(4) Li, H.; Yin, Z.; He, Q.; Li, H.; Huang, X.; Lu, G.; Fam, D. W. H.; Tok, A. I. Y.; Zhang, Q.; Zhang, H. Fabrication of Single- and Multilayer MoS_2 Film-Based Field-Effect Transistors for Sensing NO at Room Temperature. *Small* **2012**, *8*, 63−67.
(5) Wang, L.; Wang, Y.; Wong, J. I.; Palacios, T.; Kong, J.; Yang, H. Y. Functionalized MoS_2 Nanosheet-Based Field-Effect Biosensor for Label-Free Sensitive Detection of Cancer Marker Proteins in Solution. *Small* **2014**, *10*, 1101−1105.
(6) Lebègue, S.; Eriksson, O. Electronic Structure of Two-Dimensional Crystals from *ab initio* Theory. *Phys. Rev. B* **2009**, *79*, 115409.
(7) Kuc, A.; Zibouche, N.; Heine, T. Influence of Quantum Confinement on the Electronic Structure of the Transition Metal Sulfide TS_2. *Phys. Rev. B* **2011**, *83*, 245213.
(8) Splendiani, A.; Sun, L.; Zhang, Y.; Li, T.; Kim, J.; Chim, C.-Y.; Galli, G.; Wang, F. Emerging Photoluminescence in Monolayer MoS_2. *Nano Lett.* **2010**, *10*, 1271−1275.
(9) Sundaram, R. S.; Engel, M.; Lombardo, A.; Krupke, R.; Ferrari, A. C.; Avouris, P.; Steiner, M. Electroluminescence in Single Layer MoS_2. *Nano Lett.* **2013**, *13*, 1416−1421.
(10) Yin, Z. Y.; Li, H.; Jiang, L.; Shi, Y. M.; Sun, Y. H.; Lu, G.; Zhang, Q.; Chen, X. D.; Zhang, H. Single-Layer MoS_2 Phototransistors. *ACS Nano* **2012**, *6*, 74−80.
(11) Lee, G.-H.; Yu, Y.-J.; Cui, X.; Petrone, N.; Lee, C.-H.; Choi, M. S.; Lee, D.-Y.; Lee, C.; Yoo, W. J.; Watanabe, K.; Taniguchi, T.; Nuckolls, C.; Kim, P.; Hone, J. Flexible and Transparent MoS_2 Field-Effect Transistors on Hexagonal Boron Nitride-Graphene Heterostructures. *ACS Nano* **2013**, *7*, 7931−7936.
(12) Chang, H.-Y.; Yang, S.; Lee, J.; Tao, L.; Hwang, W.-S.; Jena, D.; Lu, N.; Akinwande, D. High-Performance, Highly Bendable MoS_2 Transistors with High-K Dielectrics for Flexible Low-Power Systems. *ACS Nano* **2013**, *7*, 5446−5452.
(13) Yoon, J.; Park, W.; Bae, G.-Y.; Kim, Y.; Jang, H. S.; Hyun, Y.; Lim, S. K.; Kahng, Y. H.; Hong, W.-K.; Lee, B. H.; Ko, H. C. Highly Flexible and Transparent Multilayer MoS_2 Transistors with Graphene Electrodes. *Small* **2013**, *9*, 3295−3300.
(14) Lu, W.-Y.; Taur, Y. On the Scaling Limit of Ultrathin SOI MOSFETs. *IEEE Trans. Electron Devices* **2006**, *53*, 1137−1141.
(15) Radisavljevic, B.; Radenovic, A.; Brivio, J.; Giacometti, V.; Kis, A. Single-Layer MoS_2 Transistors. *Nat. Nanotechnol.* **2011**, *6*, 147−150.
(16) Das, S.; Appenzeller, J. Where Does the Current Flow in Two-Dimensional Layered Systems? *Nano Lett.* **2013**, *13*, 3396−3402.
(17) Zhu, W.; Low, T.; Lee, Y.-H.; Wang, H.; Farmer, D. B.; Kong, J.; Xia, F.; Avouris, P. Electronic Transport and Device Prospects of Monolayer Molybdenum Disulphide Grown by Chemical Vapour Deposition. *Nat. Commun.* **2014**, *5*, 3087.
(18) Chan, M. Y.; Komatsu, K.; Li, S.-L.; Xu, Y.; Darmawan, P.; Kuramochi, H.; Nakaharai, S.; Aparecido-Ferreira, A.; Watanabe, K.; Taniguchi, T.; Tsukagoshi, K. Suppression of Thermally Activated Carrier Transport in Atomically Thin MoS_2 on Crystalline Hexagonal Boron Nitride Substrates. *Nanoscale* **2013**, *5*, 9572−9576.
(19) Min, S.-W.; Lee, H. S.; Choi, H. J.; Park, M. K.; Nam, T.; Kim, H.; Ryu, S.; Im, S. Nanosheet Thickness-Modulated MoS_2 Dielectric Property Evidenced by Field-Effect Transistor Performance. *Nanoscale* **2013**, *5*, 548−551.
(20) Das, S.; Prakash, A.; Salazar, R.; Appenzeller, J. Toward Low-Power Electronics: Tunneling Phenomena in Transition Metal Dichalcogenides. *ACS Nano* **2014**, *8*, 1681−1689.
(21) Tarasov, A.; Campbell, P. M.; Tsai, M.-Y.; Hesabi, Z. R.; Feirer, J.; Graham, S.; Ready, W. J.; Vogel, E. M. Highly Uniform Trilayer Molybdenum Disulfide for Wafer-Scale Device Fabrication. *Adv. Funct. Mater.* **2014**, *24*, 6389−6400.
(22) Das, S.; Chen, H.-Y.; Penumatcha, A. V.; Appenzeller, J. High Performance Multilayer MoS2 Transistors with Scandium Contacts. *Nano Lett.* **2012**, *13*, 100−105.
(23) Gong, C.; Colombo, L.; Wallace, R. M.; Cho, K. The Unusual Mechanism of Partial Fermi Level Pinning at Metal−MoS_2 Interfaces. *Nano Lett.* **2014**, *14*, 1714−1720.
(24) McDonnell, S.; Addou, R.; Buie, C.; Wallace, R. M.; Hinkle, C. L. Defect-Dominated Doping and Contact Resistance in MoS_2. *ACS Nano* **2014**, *8*, 2880−2888.
(25) Chuang, S.; Battaglia, C.; Azcatl, A.; McDonnell, S.; Kang, J. S.; Yin, X.; Tosun, M.; Kapadia, R.; Fang, H.; Wallace, R. M.; Javey, A. MoS_2 P-type Transistors and Diodes Enabled by High Work Function MoO_x Contacts. *Nano Lett.* **2014**, *14*, 1337−1342.
(26) Du, Y.; Yang, L.; Zhang, J.; Liu, H.; Majumdar, K.; Kirsch, P. D.; Ye, P. D. MoS_2 Field-Effect Transistors With Graphene/Metal Heterocontacts. *IEEE Electron Device Lett.* **2014**, *35*, 599−601.
(27) Lim, S. C.; Jang, J. H.; Bae, D. J.; Han, G. H.; Lee, S.; Yeo, I.-S.; Lee, Y. H. Contact Resistance between Metal and Carbon Nanotube Interconnects: Effect of Work Function and Wettability. *Appl. Phys. Lett.* **2009**, *95*, 264103.
(28) Liu, W.; Kang, J.; Sarkar, D.; Khatami, Y.; Jena, D.; Banerjee, K. Role of Metal Contacts in Designing High-Performance Monolayer n-Type WSe_2 Field Effect Transistors. *Nano Lett.* **2013**, *13*, 1983−1990.
(29) Becker, U.; Rosso, K. M.; Weaver, R.; Warren, M.; Hochella, M. F. Metal Island Growth and Dynamics on Molybdenite Surfaces. *Geochim. Cosmochim. Acta* **2003**, *67*, 923−934.
(30) Liu, W.; Kang, J.; Cao, W.; Sarkar, D.; Khatami, Y.; Jena, D.; Banerjee, K. High-Performance Few-Layer-MoS_2 Field-Effect-Transistor with Record Low Contact-Resistance. In *Electron Devices Meeting (IEDM), 2013 IEEE International, Dec 9−11, 2013*; Institute of Electrical and Electronics Engineers, Inc.: New York, 2013; pp 19.4.1−19.4.4.
(31) Baugher, B. W. H.; Churchill, H. O. H.; Yang, Y.; Jarillo-Herrero, P. Intrinsic Electronic Transport Properties of High-Quality Monolayer and Bilayer MoS_2. *Nano Lett.* **2013**, *13*, 4212−4216.
(32) Liu, H.; Si, M.; Deng, Y.; Neal, A. T.; Du, Y.; Najmaei, S.; Ajayan, P. M.; Lou, J.; Ye, P. D. Switching Mechanism in Single-Layer Molybdenum Disulfide Transistors: An Insight into Current Flow across Schottky Barriers. *ACS Nano* **2013**, *8*, 1031−1038.
(33) Kang, J.; Liu, W.; Sarkar, D.; Jena, D.; Banerjee, K. Computational Study of Metal Contacts to Monolayer Transition-Metal Dichalcogenide Semiconductors. *Phys. Rev. X* **2014**, *4*, 031005.
(34) Michaelson, H. B. The Work Function of the Elements and Its Periodicity. *J. Appl. Phys.* **1977**, *48*, 4729−4733.
(35) Gong, C.; Huang, C.; Miller, J.; Cheng, L.; Hao, Y.; Cobden, D.; Kim, J.; Ruoff, R. S.; Wallace, R. M.; Cho, K.; Xu, X.; Chabal, Y. J. Metal Contacts on Physical Vapor Deposited Monolayer MoS2. *ACS Nano* **2013**, *7*, 11350−11357.
(36) Mahatha, S. K.; Krishnakumar, S. R. M. Quantum Well States in Ag Thin Films on MoS_2 (0001) Surfaces. *J. Phys.: Condens. Matter* **2013**, *25*, 115501.
(37) Lince, J.; Carré, D.; Fleischauer, P. Schottky-barrier Formation on a Covalent Semiconductor without Fermi-level Pinning: The Metal-MoS_2(0001) Interface. *Phys. Rev. B* **1987**, *36*, 1647−1656.
(38) Ikarashi, N.; Kobayashi, K.; Hasegawa, T.; Yagi, K. Epitaxy of Au and Ag on Cleaved (10, 0) Surface of MoS_2. *Jpn. J. Appl. Phys.* **1988**, *27*, L750.
(39) Conley, H. J.; Wang, B.; Ziegler, J. I.; Haglund, R. F.; Pantelides, S. T.; Bolotin, K. I. Bandgap Engineering of Strained Monolayer and Bilayer MoS_2. *Nano Lett.* **2013**, *13*, 3626−3630.
(40) Wang, Y.; Cong, C.; Qiu, C.; Yu, T. Raman Spectroscopy Study of Lattice Vibration and Crystallographic Orientation of Monolayer MoS_2 under Uniaxial Strain. *Small* **2013**, *9*, 2857−2861.
(41) Castellanos-Gomez, A.; Roldán, R.; Cappelluti, E.; Buscema, M.; Guinea, F.; van der Zant, H. S. J.; Steele, G. A. Local Strain

Engineering in Atomically Thin MoS_2. *Nano Lett.* **2013**, *13*, 5361–5366.
(42) Lanzillo, N. A.; Glen Birdwell, A.; Amani, M.; Crowne, F. J.; Shah, P. B.; Najmaei, S.; Liu, Z.; Ajayan, P. M.; Lou, J.; Dubey, M.; Nayak, S. K.; O'Regan, T. P. Temperature-Dependent Phonon Shifts in Monolayer MoS_2. *Appl. Phys. Lett.* **2013**, *103*, 093102.
(43) Najmaei, S.; Liu, Z.; Ajayan, P. M.; Lou, J. Thermal Effects on the Characteristic Raman Spectrum of Molybdenum Disulfide (MoS_2) of Varying Thicknesses. *Appl. Phys. Lett.* **2012**, *100*, 013106.
(44) Yan, R.; Simpson, J. R.; Bertolazzi, S.; Brivio, J.; Watson, M.; Wu, X.; Kis, A.; Luo, T.; Hight Walker, A. R.; Xing, H. G. Thermal Conductivity of Monolayer Molybdenum Disulfide Obtained from Temperature-Dependent Raman Spectroscopy. *ACS Nano* **2013**, *8*, 986–993.
(45) Najmaei, S.; Ajayan, P. M.; Lou, J. Quantitative Analysis of the Temperature Dependency in Raman Active Vibrational Modes of Molybdenum Disulfide Atomic Layers. *Nanoscale* **2013**, *5*, 9758–9763.
(46) Taube, A.; Judek, J.; Jastrzębski, C.; Duzynska, A.; Świtkowski, K.; Zdrojek, M. Temperature-Dependent Nonlinear Phonon Shifts in a Supported MoS_2 Monolayer. *ACS Appl. Mater. Interfaces* **2014**, *6*, 8959–8963.
(47) Ho, C. Y.; Powell, R. W.; Liley, P. E. Thermal Conductivity of the Elements. *J. Phys. Chem. Ref. Data* **1972**, *1*, 279–421.
(48) Horcas, I.; Fernández, R.; Gómez-Rodríguez, J. M.; Colchero, J.; Gómez-Herrero, J.; Baro, A. M. WSXM: A Software for Scanning Probe Microscopy and a Tool for Nanotechnology. *Rev. Sci. Instrum.* **2007**, *78*, 013705.

NOTE ADDED AFTER ASAP PUBLICATION

This paper was posted ASAP on January 6, 2015. The Supporting Information file was replaced and the revised version was reposted on January 21, 2015.

DOI: 10.1021/am506921y
ACS Appl. Mater. Interfaces 2015, 7, 1180–1187